doi:10.1016/j.jmb.2009.07.087 J. Mol. Biol. (2009) 392, 1266–1277

JMB

Available online at www.sciencedirect.com

ScienceDirect

ELSEVIER

Structural Basis of Substrate Specificity of Plant 12-Oxophytodienoate Reductases

Constanze Breithaupt[1]*, Robert Kurzbauer[2], Florian Schaller[3], Annick Stintzi[4], Andreas Schaller[4], Robert Huber[5,6,7], Peter Macheroux[8] and Tim Clausen[2]*

[1]*Institute of Biochemistry and Biotechnology, Martin-Luther-University Halle-Wittenberg, Kurt-Mothes-Str. 3, 06120 Halle, Germany*

[2]*Research Institute of Molecular Pathology (IMP), Dr. Bohrgasse 7, 1030 Vienna, Austria*

[3]*Lehrstuhl für Pflanzenphysiologie, Ruhr-Universität Bochum, Universitätstr. 150, 44801 Bochum, Germany*

[4]*Institute of Plant Physiology and Biotechnology (260), University of Hohenheim, Emil-Wolff-Str. 25, 70593 Stuttgart, Germany*

[5]*Max-Planck-Institut für Biochemie, Am Klopferspitz 18, 82152 Martinsried, Germany*

[6]*School of Biosciences, University of Cardiff, Cardiff CF10 3TL, UK*

[7]*Zentrum für medizinische Biotechnologie, Universität Duisburg-Essen, 45117 Essen, Germany*

[8]*Institute of Biochemistry, Graz University of Technology, 8010 Graz, Austria*

12-Oxophytodienoate reductase 3 (OPR3) is a FMN-dependent oxidoreductase that catalyzes the reduction of the cyclopentenone (9*S*,13*S*)-12-oxophytodienoate [(9*S*,13*S*)-OPDA] to the corresponding cyclopentanone in the biosynthesis of the plant hormone jasmonic acid. *In vitro*, however, OPR3 reduces the jasmonic acid precursor (9*S*,13*S*)-OPDA as well as the enantiomeric (9*R*,13*R*)-OPDA, while its isozyme OPR1 is highly selective, accepting only (9*R*,13*R*)-OPDA as a substrate. To uncover the molecular determinants of this remarkable enantioselectivity, we determined the crystal structures of OPR1 and OPR3 in complex with the ligand *p*-hydroxybenzaldehyde. Structural comparison with the OPR1:(9*R*,13*R*)-OPDA complex and further biochemical and mutational analyses revealed that two active-site residues, Tyr78 and Tyr246 in OPR1 and Phe74 and His244 in OPR3, are critical for substrate filtering. The relatively smaller OPR3 residues allow formation of a wider substrate binding pocket that is less enantio-restrictive. Substitution of Phe74 and His244 by the corresponding OPR1 tyrosines resulted in an OPR3 mutant showing enhanced, OPR1-like substrate selectivity. Moreover, sequence analysis of the OPR family supports the filtering function of Tyr78 and Tyr246 and allows predictions with respect to substrate specificity and biological function of thus far uncharacterized OPR isozymes. The discovered structural features may also be relevant for other stereoselective proteins and guide the rational design of stereospecific enzymes for biotechnological applications.

**Corresponding authors.* E-mail addresses: constanze.breithaupt@biochemtech.uni-halle.de; clausen@imp.univie.ac.at.

Abbreviations used: OPR, 12-oxophytodienoate reductase; OPDA, 12-oxophytodienoate; JA, jasmonic acid; PHB, *p*-hydroxybenzaldehyde; OYE, old yellow enzyme; PEG, polyethylene glycol; GC–MS, gas chromatography–mass spectrometry; DH-OPDA, dihydro-OPDA.

0022-2836/$ - see front matter

Received 14 May 2009;
received in revised form
27 July 2009;
accepted 29 July 2009
Available online
4 August 2009

Edited by M. Guss

Keywords: OPR; oxyphytodienoate reductase; jasmonic acid; enantioselectivity; old yellow enzyme

Introduction

12-Oxophytodienoate reductases (OPRs) are a small group of flavin-dependent oxidoreductases in plants related to old yellow enzyme (OYE) from *Saccharomyces cerevisiae*.[1,2] Their name is derived from OPR3 in *Solanum lycopersicum* (tomato) and *Arabidopsis thaliana* (thale cress), which catalyzes the reduction of the cyclopentenone (9*S*,13*S*)-12-oxophytodienoate [(9*S*,13*S*)-OPDA] to the corresponding cyclopentanone (Fig. 1a) in the biosynthesis of jasmonic acid (JA).[3,4] JA and its derivatives constitute a family of plant hormones, collectively called jasmonates, which serve multiple roles in plant defense and development. Initially known for their growth-inhibitory and senescence-promoting activities, jasmonates are now well

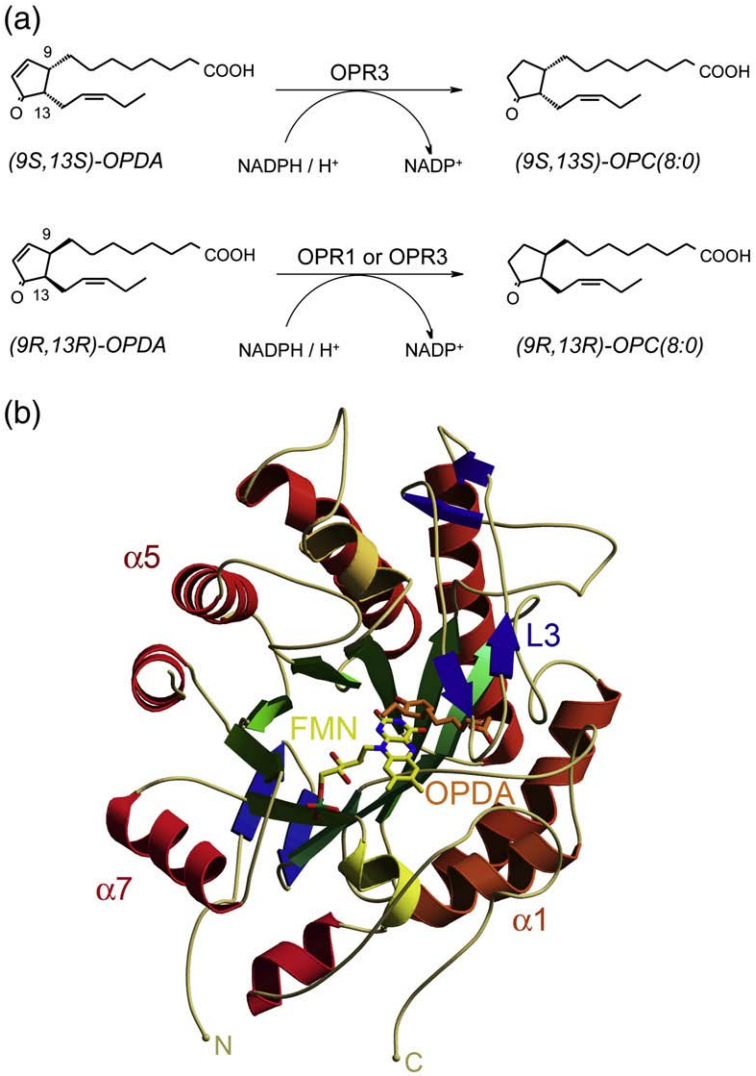

Fig. 1. Reactivity and structure of OPRs. (a) Scheme of the substrate specificity of OPR isoforms. Whereas OPR3 reduces both *cis*-OPDA enantiomers, OPR1 only reduces (9*R*,13*R*)-OPDA. (b) Ribbon diagram of the *Sl*OPR1 structure in complex with (9*R*,13*R*)-OPDA. FMN (yellow) and (9*R*,13*R*)-OPDA (orange) are shown as stick models. Secondary structures complementing the $\alpha_8\beta_8$ barrel are shown in blue.

established as signalling molecules in plant resistance responses against herbivores and pathogens, as well as numerous developmental processes including male and female reproductive development, the formation of tubers and glandular trichomes, tendril coiling, lacticifer differentiation, and seed germination.[5]

The requirement of OPR3 for JA biosynthesis is evident from the *OPR3* single-gene loss-of-function mutant in *Arabidopsis*, which is jasmonate deficient, male sterile, and impaired in jasmonate-dependent gene expression.[6,7] Consistent with the genetic data, the biochemical characterization of recombinant OPRs revealed that OPR3 in tomato and *Arabidopsis* and OPR3 orthologs in other species are unique in their ability to reduce (9*S*,13*S*)-OPDA, which is the only precursor of biologically active JA among the four possible OPDA stereoisomers.[8–10] The characterization of different OPR isoforms allowed to distinguish two types of activities with respect to their specificity for OPDA stereoisomers: OPR3-like enzymes exhibit a relaxed substrate specificity and reduce both the (9*S*,13*S*)- and the (9*R*,13*R*)-enantiomers of OPDA. In contrast, OPR1-like enzymes are highly selective, accepting only (9*R*,13*R*)-OPDA as a substrate (Fig. 1a).

Like all members of the OYE family, OPR1 and OPR3 from *S. lycopersicum* and from *A. thaliana* exhibit the frequently observed $(\alpha/\beta)_8$ barrel fold, in which the cylindrical eight-stranded parallel β-sheet is surrounded by eight α-helices (Fig. 1b).[11–14] The FMN cofactor is bound noncovalently at the C-terminal end of the β-barrel, where loops L1–L8 (loops are numbered according to the preceding β-strand, e.g., L8 follows β8) set up the active-site cavity above the FMN and the substrate specificity regions. The characteristic enzymatic feature of the OYE family is the ability to hydrogenate the olefinic bond of α,β-unsaturated carbonyl compounds. The reaction has been shown to proceed via a ping-pong bi-bi mechanism including NAD(P)H binding, reduction of FMN, release of $NAD(P)^+$, substrate binding, and reduction.[15,16] The carbonyl group of the α,β-unsaturated carbonyl substrate is fixed and oriented above the FMN by two strong hydrogen bonds to a conserved His/His or His/Asn pair that simultaneously activates the substrate's olefinic bond for hydride transfer from the reduced flavin. In most of the OYE family members, a tyrosine is positioned above the substrate that has been shown to act as the proton donor during substrate reduction in OYE.[17]

In the *Sl*OPR1:(9*R*,13*R*)-OPDA complex structure, the cyclopentenone ring of OPDA binds into a small cavity above the FMN, where it is oriented by

Table 1. Data collection and refinement statistics

	OPR1:PHB	OPR3:PHB	OPR3YY
Data collection			
Space group	*P*1	$P2_1$	$P2_1$
Unit cell dimensions [Å]	$a=53.44$, $b=71.99$, $c=72.04$, $\alpha=63.09°$, $\beta=84.45°$, $\gamma=78.06°$	$a=57.612_1$, $b=89.50$, $c=80.68$, $\alpha=90.0°$, $\beta=107.94°$, $\gamma=90.0°$	$a=49.142_1$, $b=92.86$, $c=89.62$, $\alpha=90.0°$, $\beta=98.08°$, $\gamma=90.0°$
Resolution [Å][a]	2.3 (2.34–2.30)	2.0 (2.00–2.07)	2.3 (2.38–2.30)
Observed reflections	77,324	120,545	54,312
Independent reflections	40,037	49,387	32,400
Completeness [%]	97.1 (80.1)	93.9 (89.4)	91.6 (89.9)
R_{merge} [%][b]	5.6 (20.0)	8.1 (38.9)	11.4 (41.1)
$\langle I\rangle/\langle\sigma(I)\rangle$	13.4 (2.7)	10.6 (2.0)	9.1 (2.1)
B value of Wilson plot [Å^2]	35.7	26.7	..
Refinement			
R_{cryst}/R_{free} [%][c]	20.3/25.4	20.6/23.7	20.1/25.8
No. of atoms			
Protein/FMN	5546/62	5653/62	5657/62
Ligand/water	18/292	18/375	0/501
Rmsd			
Bonds [Å]	0.008	0.006	0.006
Angles [°]	1.35	1.21	1.22
Bonded *B*'s [Å^2][d]	2.34	1.42	1.91
Mean *B* value [Å^2]			
Protein/FMN	34.4/28.8	27.0/22.8	34.5/31.3
Ligand/water	37.7/36.1	25.1/30.7	—/42.8
Ramachandran plot [%]			
Most favored	88.3	88.8	87.6
Additional allowed	11.7	11.0	12.4
Generously allowed	0	0.2	0
Disallowed	0	0	0

[a] Values in parentheses correspond to the highest-resolution shell.
[b] $R_{merge}=\sum_{hi}|I_i(h)-\langle I(h)\rangle|/\sum_{hi}I_i(h)$.
[c] $R_{cryst}=\sum_h||F_o(h)|-|F_c(h)||/\sum_h|F_o(h)|$. R_{free} was determined from 5% of the data that were not used for refinement.
[d] Rmsd of bonded *B*'s: rmsd of temperature factors of bonded atoms.

hydrogen bonds to His187 and His190 for hydride transfer from the cofactor and for protonation by Tyr192.[11] The substrate is further fixed by its carboxy alkyl chain binding into a tunnel formed by loop L3 of *Sl*OPR1 (Fig. 1b).

Despite the high degree of sequence identity between OPR1 and OPR3 (*Sl*OPR1/*Sl*OPR3: 55.5% for 375 aligned residues), the structural similarity (rmsd: 0.86 Å for 342 aligned Cαs), as well as the strict conservation of all residues in the interior of the active-site cavity, OPR1 and OPR3 differ remarkably in their ability to reduce the four stereoisomers of OPDA. To uncover the molecular determinants that underlie this difference in substrate stereoselectivity, we have determined the structures of *Sl*OPR1 and *Sl*OPR3 complexed with *p*-hydroxybenzaldehyde (PHB) as a substrate analogue. Biochemical and structural analysis of several site-directed mutants revealed two active-site residues that are critical for substrate specificity in the family of OPR enzymes.

Results and Discussion

Complex formation of *para*-hydroxybenzaldehyde with OPR1 and OPR3

To study the molecular parameters that underlie the distinct substrate preferences of OPR1 and OPR3, we aimed to analyze the structure of OPR1 and OPR3 from *S. lycopersicum* in complex with substrate (when not otherwise mentioned, OPR1 and OPR3 refer to the *S. lycopersicum* enzymes). As reported previously, the OPR1:(9*R*,13*R*)-OPDA complex was determined at high resolution by soaking OPR1 crystals with substrate.[11] However, OPR3 crystallizes as a self-inhibited dimer, in which the substrate binding pocket is occupied by loop L6 of the neighboring protomer.[12] This may explain the failure to soak the OPDA substrate into OPR3 crystals. Since co-crystallization trials were also not successful, we tried to obtain a complex structure with the ligand PHB, which forms a charge-transfer complex with FMN, characteristic for the OYE family.[18–20] PHB was chosen because of its good solubility and (i) it is a cyclic compound like OPDA; (ii) binding of its oxyanion in the OYE:PHB complex resembles binding of the OPDA carbonyl group in the OPR1:(9*R*,13*R*)-OPDA complex; and (iii) its aldehyde substitution in *para* position extends the phenol ring comparable to the alkyl chains in OPDA. We soaked the OPR3 crystals in a crystallization solution saturated with PHB (>100 mM) and determined the structure of the resulting OPR3:PHB complex by molecular replacement at 2.0-Å resolution (Table 1). In parallel, we solved the crystal structure of the OPR1:PHB complex at 2.3-Å resolution (Table 1). In both structures, the PHB ligand is well defined by electron density (Fig. 2a) and allowed a direct comparison of ligand binding in OPR1 and OPR3.

In the OPR1 complex structure, the orientation of PHB closely resembles that of (9*R*,13*R*)-OPDA (Fig. 2b). The hydroxy oxygen of PHB, which has been shown to be deprotonated in the OYE:PHB complex,[19] is positioned at exactly the same position as the substrate's carbonyl oxygen and forms strong hydrogen bonds to His187 and His190. In the OPR1:(9*R*,13*R*)-OPDA complex, these hydrogen bonds serve to orient and activate OPDA for hydride transfer. The aromatic ring of PHB forms stacking interactions with the isoalloxazine ring of the FMN comparable to the cyclopentenone ring of OPDA, and the aldehyde group of PHB mimics the carboxy alkyl chain of OPDA by binding to the tunnel in the specificity region of OPR1. In OPR3, PHB is bound in a similar arrangement above the FMN, with its hydroxy oxygen being in close contact to the two catalytic histidine residues (Fig. 2c). However, one obvious difference is the orientation of the aromatic ring of PHB relative to the FMN isoalloxazine ring. In OPR1, the PHB ring is tilted about 15° against the flavin ring system, whereas in the OPR3:PHB complex, both ring systems are arranged parallel with each other. The different orientation correlates with a slight shift of the entire ligand towards the protein interior in OPR1 thereby anchoring it more deeply in the active-site pocket. The distinct PHB binding modes can be explained by several structural features: (1) Whereas in OPR1 the bulky Tyr246 forms part of the entrance of the substrate binding pocket, OPR3 employs the relatively smaller His244 yielding a larger and sterically less restrictive binding cavity. (2) In OPR1, a parallel arrangement of PHB and FMN is precluded by Tyr358 that extends directly above one of the FMN methyl groups towards the active-site cavity. In contrast, the equivalent Tyr370 of OPR3 is shifted slightly to a more remote region thereby freeing additional space above the FMN cofactor needed for parallel stacking interactions of FMN and PHB. Moreover, Tyr370 is in the proper position to allow the formation of a short-distanced (2.5 Å) hydrogen bond between its hydroxy group and the aldehyde group of the PHB. (3) Unlike in OPR1, PHB is bound to the FMN of OPR3 via its *si*-face, resulting in the observed opposite orientation of the aldehyde group. This binding mode is enforced by Phe74 of OPR3. Whereas its OPR1 counterpart (Tyr78) forms part of the ceiling at the entrance of the cavity, Phe74 is shifted slightly downwards with its phenyl group rotated towards the inner cavity, thereby preventing formation of an OPR1-like specificity tunnel for the substrate's alkyl chain. Simultaneously, this rotation increases the size of the cyclopentenone binding pocket. In sum, the structural data suggest that the gatekeeping OPR3 residues Phe74 and His244 (Tyr78 and Tyr246 in OPR1) together with Tyr370 (Tyr358 in OPR1) determine the binding mode of PHB and might thus be critical factors for substrate specificity.

Stereoselectivity of the OPR double mutant Phe74Tyr/His244Tyr

To probe the role of Phe74 and His244 as a substrate filtering device, an enzyme–substrate complex of OPR3 and (9*R*,13*R*)-OPDA was modeled. To this

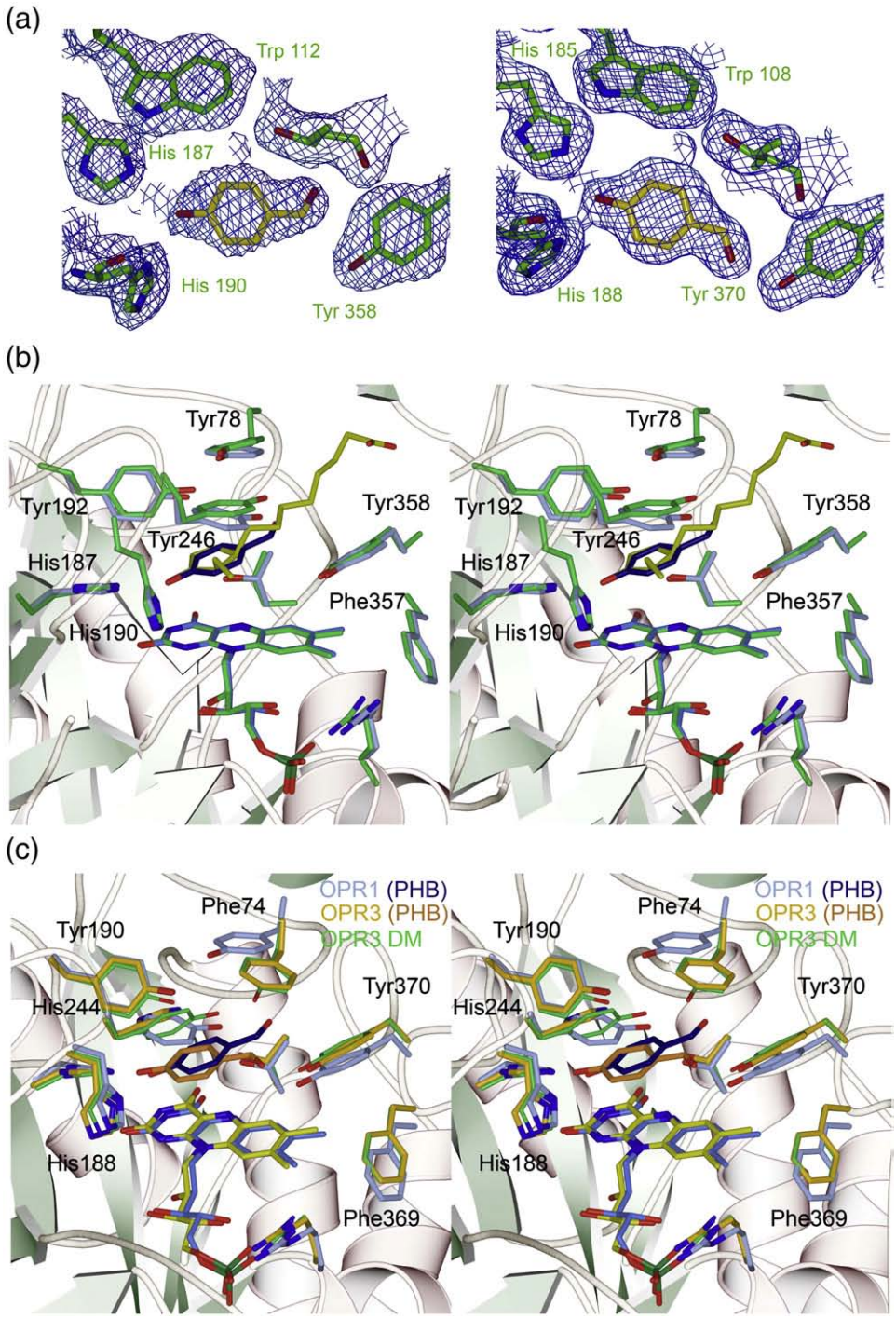

Fig. 2. Binding of PHB to OPR1 and OPR3. (a) $2F_o - F_c$ omit electron density map of the complex structures of OPR1:PHB (left) and OPR3:PHB (right), at 2.30- and 2.07-Å resolution, contoured at 1.0σ. For map calculation, PHB was omitted from the model. (b) Stereo view of the superposition of the active-site cavities of OPR1:PHB (light blue) and OPR1:(9*R*,13*R*)-OPDA (green). The PHB ligand is shown in dark blue and OPDA in yellow. In addition, the ribbon structure of OPR1 is shown. (c) Stereo view of the superposition of the active-site cavities of OPR1:PHB (light blue), OPR3:PHB (yellow), and the OPR3 double mutant OPR3YY (green). The PHB ligand is shown in dark blue (OPR1) and orange (OPR3). In addition, the ribbon structure of OPR3 is shown. Residues are numbered according to the OPR3 sequence.

end, the OPR1:(9*R*,13*R*)-OPDA structure was superimposed onto OPR3 and then used as a template from which the coordinates of the OPDA substrate were transferred to the active site of OPR3 (Fig. 3). Comparison of both structures illustrated the particular importance of the two gatekeeping residues. In the OPR1:(9*R*,13*R*)-OPDA complex structure, Tyr78 and Tyr246 delimit the narrow substrate binding cavity in which the cyclopentenone ring, including the two stereo centers, as well as the neighboring C8 and C14 methylene groups of the extending alkyl chains, is completely buried (Fig.

3a). In contrast, the entrance to the active-site cavity of OPR3, which is bordered by the relatively smaller Phe74 and His244, is much wider. In the modeled substrate complex, the cyclopentenone ring is less buried and the position of the stereo centers is less restricted than in OPR1 (Fig. 3b). Therefore, the modeling studies support the assumption that the two smaller gatekeeping residues are responsible for the broader substrate specificity of OPR3.

To test this hypothesis, we generated the two OPR3 mutants Phe74Tyr and His244Tyr as well as the double mutant Phe74Tyr/His244Tyr (OPR3YY), which is predicted to confer an OPR1-like substrate specificity to OPR3. The mutant enzymes were expressed in *Escherichia coli* and analyzed with respect to their ability to reduce (9*S*,13*S*)-OPDA (Fig. 4). Both the Phe74Tyr and the His244Tyr single mutants were similarly impaired in the reduction of (9*S*,13*S*)-OPDA, and the reaction was even slower in the Phe74Tyr/His244Tyr double mutant (Fig. 4a). These findings are consistent with the interpretation of the structural data suggesting that the bulkier tyrosine residues impair proper binding of the (9*S*,13*S*)-enantiomer to the OPR3 active-site cavity. To test whether the impaired reduction of (9*S*,13*S*)-OPDA by the site-directed OPR3 mutants is due to an overall loss of enzymatic activity, or else, an enhanced stereoselectivity for the (9*R*,13*R*)-enantiomer, the recombinant enzymes were analyzed with a racemic mixture of (9*S*,13*S*)-OPDA and (9*R*,13*R*)-OPDA as the substrate. The reaction was stopped after 30 min and the relative consumption of the two stereoisomers was analyzed. In contrast to wild-type OPR3, for which each of the two isomers represented 50% of all the substrate consumed, the single and double mutants showed a clear preference for (9*R*,13*R*)-OPDA over (9*S*,13*S*)-OPDA (Fig. 4b). Apparently, replacement of Phe74

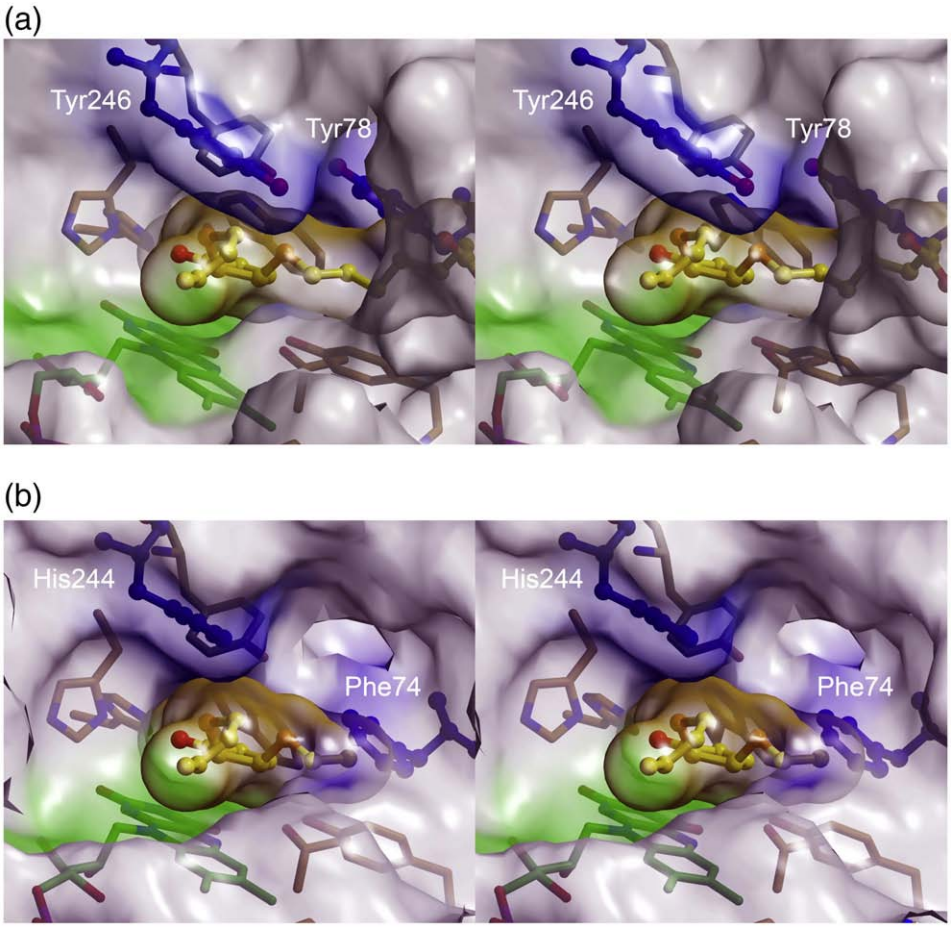

Fig. 3. Substrate binding to OPR1 and OPR3. (a) Stereo view of the active-site cavity of the OPR1:(9*R*,13*R*)-OPDA complex. In addition to the molecular surfaces of OPR1 (grey; surface of FMN: green) and of the substrate (9*R*,13*R*)-OPDA (yellow), Tyr246 and Tyr78 that narrow the opening of the cavity as well as (9*R*,13*R*)-OPDA are shown as ball-and-stick models (blue). (b) Stereo view of the active-site cavity of a modeled OPR3:(9*R*,13*R*)-OPDA complex. Surfaces were colored as in (a). The complex was obtained by transferring the substrate's coordinates of the aligned OPR1:(9*R*,13*R*)-OPDA complex to the OPR3 structure. Protein residues of OPR3 and the substrate's carboxy alkyl chain (shortened in the figure for clarity) clash in the model because OPR3 lacks the tunnel that accommodates the carboxy alkyl chain in OPR1. In OPR3, these clashes can be easily avoided by a change in the conformation of atoms C1 to C8 of the carboxy alkyl chain. In comparison to OPR1, the opening of the OPR3 cavity is lined by His244 and Phe74, resulting in a wider entrance and leaving more space near the stereo centers of the substrate.

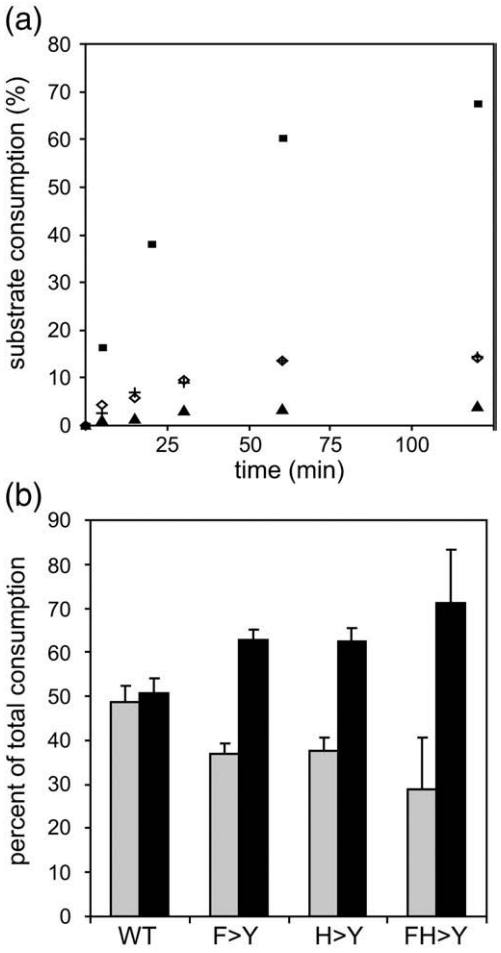

Fig. 4. Substrate specificity of site-directed OPR3 mutants. (a) Reduction of (9*S*,13*S*)-OPDA by OPR3 wild-type enzyme and site-directed mutants. The rate of (9*S*,13*S*)-OPDA (0.1 mM) reduction was compared for the OPR3 wild-type enzyme (wt, ■) and the site-directed mutants His244Tyr (+) and Phe74Tyr (♦) and the double mutant Phe74Tyr/His244Tyr (▲). At the indicated time points, the reactions were stopped and the reaction product dihydro-OPDA (DH-OPDA) was quantified by GC–MS. Product formation is given in percent of the initial amount of substrate. The data points represent the mean of two experiments. (b) Stereoselectivity of OPR3 wild-type enzyme and site-directed mutants. Racemic *cis*-OPDA (0.2 mM) was offered as substrate to the wild-type form of *SlOPR3* (wt) and to site-directed mutants. The relative consumption of (9*S*,13*S*)-OPDA (gray bars) and (9*R*,13*R*)-OPDA (black bars) was analyzed after 30 min by GC–MS and is indicated as percent of the total amount of substrate reduced. In three experiments, with enzyme concentrations ranging from 1 to 100 μg/ml, the total amount of substrate that was consumed during the 30-min reaction increased with the enzyme concentration (not shown). Regardless of the enzyme concentration, a similar increase in stereoselectivity was observed for the mutant as compared to the wild-type enzymes. The data represent the mean of the three experiments, and error bars indicate the SD.

and His244 of OPR3 by the corresponding residues of OPR1 resulted in an enhanced substrate enantioselectivity as observed for OPR1.

To investigate the structural basis of the increased selectivity, we crystallized OPR3YY and determined the structure at 2.3-Å resolution (Supplementary Fig. S1; Table 1). Interestingly, the protein crystallized as a monomer with none of the dimer interactions retained. Loop L6, which blocks the active site of the molecular neighbor in wild-type OPR3, was flexible and not defined by electron density in OPR3YY. Overall, the structure of OPR3YY was more similar to the structures of the monomeric Tyr364Phe and Glu291Lys mutants[12] than to the wild-type OPR3. The rms deviations for 358–367 Cαs were 0.18, 0.19, and 0.30 Å, respectively. Structural alignment of wild-type OPR3 and OPR3YY showed that replacement of His244 by tyrosine prevents binding of loop L6 to the substrate binding cavity, which is a prerequisite for dimerization in OPR3. The introduced tyrosine side chain would clash with Glu291 of loop L6 of the partner protomer and thus impedes the interaction of this glutamate with the two active-site histidines His185 and His188. As was shown for the Glu291Lys mutant, these interactions are essential for anchoring loop L6 in the substrate binding pocket of the molecular neighbor.[12] Otherwise, the introduced tyrosines did not induce significant rearrangements of the protein backbone and retained the same orientation as the original residues (Fig. 2c). However, the two tyrosines are much bulkier and therefore restrict the opening of the active site significantly. Together with Tyr190, they are arranged in a triangular fashion and form the ceiling of the substrate binding pocket. The three hydroxy groups are located in the center of the tyrosine triad and interact with each other via a wedged water molecule. Particularly, the tyrosine replacing His244 narrows the space in the cyclopentenone binding site and should restrict the possible configurations of the alkyl chains of the OPDA substrate (Fig. 2c). Thus, the structural data indicate that tightening of the substrate binding pocket by introducing the relatively bulkier tyrosine residues enhances the stereoselectivity of OPR3, although it does not allow to fully discriminate between (9*R*-13*R*)-OPDA and (9*S*-13*S*)-OPDA enantiomers.

Another feature expected to influence substrate specificity is the OPR1 binding site for the carboxy alkyl chain of the OPDA substrate. This alkyl chain is bound in a hydrophobic tunnel, where it makes numerous van der Waals contacts with bordering hydrophobic residues, predominantly with the aromatic rings of Tyr78 and Tyr358, which sandwich the substrate's carboxy alkyl chain. Due to the different orientation of Phe74, the OPR3 equivalent of Tyr78 in OPR1, and the different conformation of loop L3, this tunnel is not formed in OPR3. In the OPR3YY double mutant, the Tyr74 side chain retains the OPR3-typical conformation and continues to block access to the specificity region that anchors the OPDA carboxy alkyl chain in OPR1. The importance of the conformation of this aromatic residue is corroborated by the recent discovery of isozyme-specific stereocontrol in the reduction of 1-nitro-2-phenylpropene by OPR1 and OPR3.[21] Docking of the small prochiral nitroalkene indicated

that the different orientation of Phe74 in OPR1 and Tyr78 in OPR3 determines the substrate binding mode in the active site resulting in opposite enantiomeric products.[21] Therefore, the active site of OPR3YY combines characteristics of both OPR1 and OPR3 active sites, allowing partial distinction between different OPDA enantiomers.

The present structures also illustrate a further, more general feature important for stereospecific catalysis. Ligand binding to OPR1 and OPR3 solely induces minor adjustments in the individual active sites, pointing to a rigid, quasi pre-formed substrate binding pocket. This rigidity might be crucial to avoid binding of the "wrong" isomer, which could

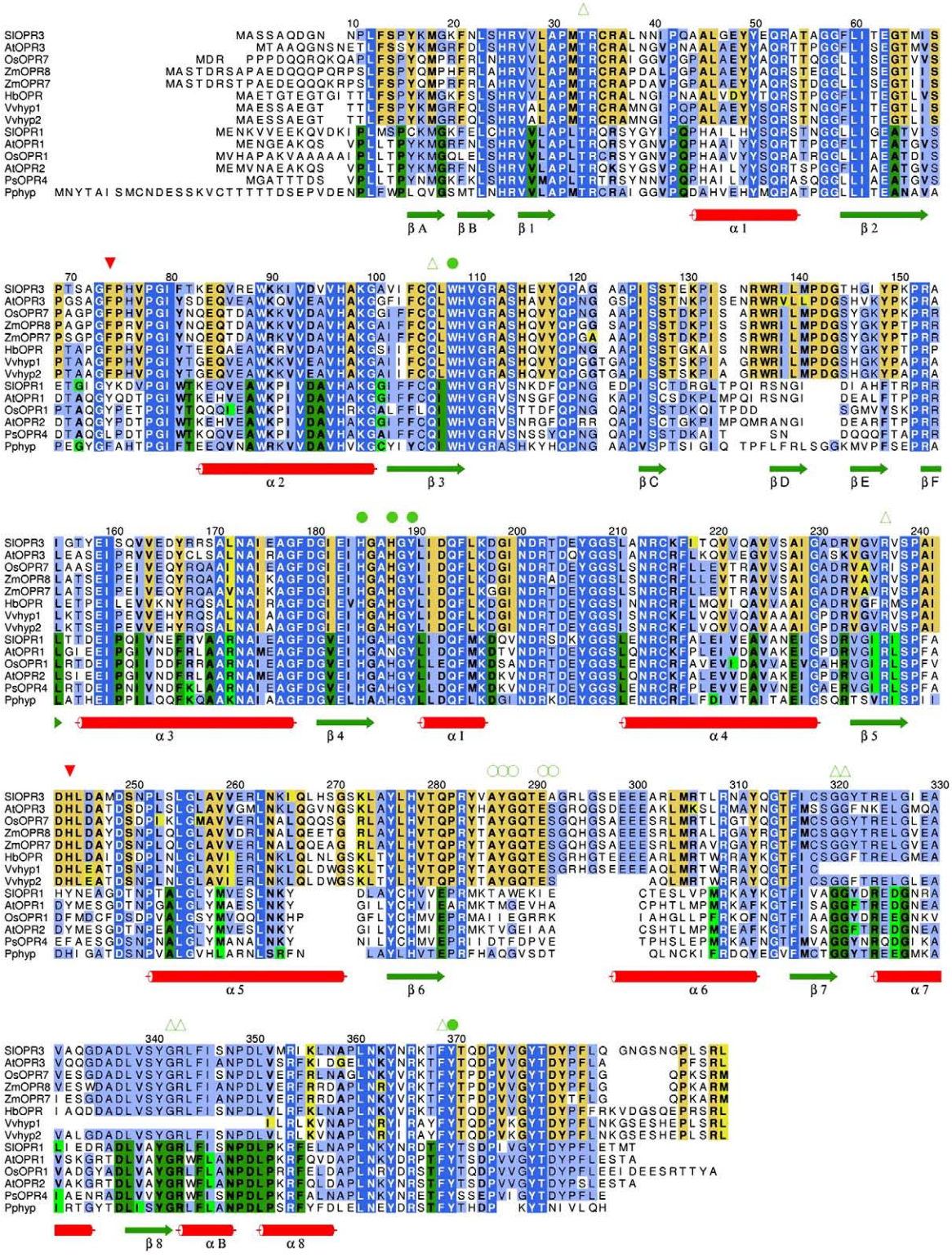

Fig. 5 (*legend on next page*)

be eased by a plastic, flexible active site. In OPR1, the rigidity of the active site is supported by an extensive hydrogen-bonding network, including Asn247, Gln140, Tyr192, and Tyr78. The rigidity of both OPR active sites is also evident from the analysis of thermal motion factors, as the *B*-factors of the substrate binding residues are significantly smaller than the average *B*-factor of all protein residues [OPR3:PHB, 15.2 Å^2 in active-site cavity, 20.9 Å^2 in average; OPR3(Glu291Lys) (active site filled with water), 15.5 and 19.4 Å^2; OPR1:PHB, 31.2 and 34.2 Å^2; OPR1, 35.2 and 37.9 Å^2].

Determinants of substrate specificity within the OPR family

Based on phylogenetic analyses, the family of OPR-like plant enzymes can be divided into two subgroups.[22–24] All OPR enzymes that, like OPR3, are able to reduce the JA precursor (9*S*,13*S*)-OPDA (*At*OPR3,[8] *Sl*OPR3,[9] and *Os*OPR7[10]) belong to subgroup II, whereas enzymes exhibiting the pronounced OPR1-like substrate specificity are found in subgroup I (*At*OPR1, *At*OPR2,[8] *Sl*OPR1,[9] and *Os*OPR1[22]). Throughout both subgroups, residues fixing the FMN cofactor are extensively conserved, as are the catalytic His/His (His/Asn) pair and the proton donor Tyr190 (Fig. 5). In addition, Trp108 and Thr33 within the active-site cavity are conserved in most of the OPR-like enzymes.

A characteristic feature of all enzymes of subgroup II is a seven-residue extension of loop L6 that is critical for dimer formation of OPR3. With the single exception of Ala292, all the L6 residues contributing to the dimerization interface are strictly conserved in subgroup II but do not exist in subgroup I (Fig. 5). The present findings identified two further residues, Phe74 and His244, as a subgroup II signature motif that is required to reduce the JA precursor (9*S*,13*S*)-OPDA. The strict conservation of this motif suggests that hitherto biochemically uncharacterized members of OPR subgroup II will also be able to reduce (9*S*,13*S*)-OPDA and thereby take part in JA biosynthesis (Fig. 5).

In the majority of OPR enzymes of subfamily I, these two residues are replaced by two tyrosines, corresponding to Tyr78 and Tyr246 in OPR1. The six OPR genes of *P. sativum* that have been identified so far all belong to subgroup I.[23] Interestingly, Tyr78 and Tyr246 are not conserved in the isozymes *Ps*OPR4 and *Ps*OPR5. Whereas *Ps*OPR5 might be a silenced pseudogene, *Ps*OPR4 expression is induced by different cues (e.g., by the JA mimic coronatine or leaf detachment), and recombinantly produced *Ps*OPR4 actively reduces 2-cyclohexen-1-one. In *Ps*OPR4, Tyr78 and Tyr246 are substituted by two smaller residues (Leu and Phe, respectively), which is predicted to result in a wider opening of the substrate binding cavity as in OPR3. Therefore, *Ps*OPR4 is a candidate enzyme for the reduction of (9*S*,13*S*)-OPDA in the pathway for JA biosynthesis in pea. Similarly, the recently sequenced genome of *P. patens*[26] contains seven OPR-like genes, none of which belongs to subgroup II. Yet, in five of the seven predicted gene products, Tyr246 is replaced by a smaller residue. In one of the five, the second gatekeeping residue (Tyr78) is replaced by phenylalanine and can thus be identified as a candidate for an OPR3-like activity for JA biosynthesis (Fig. 5).

Conclusion

OPRs are flavoenzymes that can reduce a concise set of substituted cyclopentenones differing only in the chirality of their two substituted ring carbons. Thereby, different OPR isozymes exhibit clearly defined and distinct substrate stereoselectivities, although they show a high sequence identity and employ a conserved set of catalytic residues to hydrogenate the olefinic Cα–Cβ bond of their substrates. Consequently, substrate specificity appears to be determined by a few key residues in the active site. The present study aimed to identify these molecular determinants using OPR1 and OPR3 from tomato as a model system. Following a structural–biochemical approach, we identified two active-site residues that function as a substrate filter and enable OPR enzymes to distinguish between the (9*R*,13*R*)-OPDA and (9*S*,13*S*)-OPDA enantiomers. Mutation of these two key residues conveyed OPR1-like stereoselectivity to the unspecific OPR3 enzyme. Subsequent sequence analysis of OPR enzymes from different organisms indicated their general specificity-determining role. We showed that these residues delimit the size of the active-site cavity, in particular its entrance region, and thus contribute essentially to the selection of substrates. The structural data further suggest that this ligand binding pocket is a comparably rigid structure

Fig. 5. Multiple amino acid sequence alignment of OPR1- and OPR3-like enzymes. Enzymes that belong to OPR subgroup II are shown in the upper rows of the alignment (*Os*OPR7: *Oryza sativa* OPR7 according to Tani *et al.*[10] *Os*OPR13,[25] Os08g0459600; *Zm*OPR8: *Zea mays* OPR8, gi|162462945; *Zm*OPR7: gi|162460824; *Hb*OPR: *Hevea brasiliensis* OPR, gi|63029722; *Vv*hyp1: *Vitis vinifera* hypothetical protein, gi|147781156; *Vv*hyp2: *V. vinifera* unnamed protein product, gi|157342548). Enzymes of subgroup I (*Os*OPR1: Os06g0216300; *Pisum sativum* OPR4:Q76FR8) as well as an OPR-like hypothetical protein from *Physcomitrella patens* (gi|162681370) are shown below. The secondary structural elements of *Sl*OPR3 are depicted below the alignment. Residues that are strictly conserved through both subgroups are shaded in blue; well-conserved residues are in light blue. Residues that are strictly conserved in subgroup II or I are shaded in orange or green, respectively, and conservatively substituted residues are in yellow or light green, respectively. The two specificity-determining residues Phe74/Tyr78 and His244/Tyr246 are marked by red arrows. Residues involved in substrate binding and catalysis (marked by a green filled circle) and residues important for FMN binding (marked by an open triangle) are completely conserved in all sequences, except for *Vv*hyp1. Additionally, among subgroup II enzymes, residues that bind to the substrate binding cavity of their dimerization partner in *Le*OPR3 (marked by an open circle) are completely conserved.

able to discriminate between closely related substrate molecules.

OPR1 and OPR3 are interesting candidates for asymmetric catalysis as they are able to asymmetrically reduce various activated alkenes with high, in part complementary, enantiomeric excess.[21,27,28] Our results show that directed mutagenesis of the gatekeeping residues Phe74 and His244 leads to a change in substrate specificity while retaining enzyme activity, and thus represent a valuable starting point for enlarging the range of possible substrates and eventually the enantiomeric excess for biotechnological use. In addition, mutation of these two residues is a promising strategy when trying to enhance substrate enantioselectivity of non-prochiral substrates such as OPDA, which would allow the use of OPR enzymes for the chiral separation of enantiomers by enzymatic resolution.

Materials and Methods

Crystallization of the OPR3YY mutant and OPR complexes with PHB

OPR1 and OPR3 were expressed and purified as described previously.[12,29] The OPR3YY double mutant was generated using the QuikChange Site-Directed Mutagenesis Kit (Stratagene) and verified by sequencing. The mutant was purified using the same protocol as for the wild-type protein. All crystallization trials were carried out in Cryschem plates (reservoir volume of 500 μl) at 19 °C using the sitting-drop vapor diffusion method. Crystals of wild-type OPR3 were grown by mixing 3 μl of protein with 1.5 μl of a crystallization solution containing 100 mM Mes/Tris (pH 6.5), 16% polyethylene glycol (PEG)-8000, and 50 mM ammonium sulfate. For structural analysis of the OPR3:PHB complex, it was essential to soak crystals in a saturated solution. Thus, the PHB inhibitor was added in solid form to a crystallization drop containing freshly grown crystals of OPR3. The crystals were incubated overnight until a color change from yellow to red indicated the formation of a charge-transfer complex between FMN and PHB.[19,20] Crystals of OPR1 were grown as described previously.[11] For generation of the OPR1:PHB complex, crystals of OPR1 were soaked in PEG400-free crystallization solution and then transferred to PEG400-free crystallization solution complemented with 10 mM PHB. Crystals of the OPR3YY double mutant were grown in 96-well plates (100 μl reservoir) by mixing 200 nl of protein (25 mg/ml) with 100 nl of crystallization solution containing 1 M $(NH_4)_2HPO_4$, 0.1 M sodium acetate (pH 4.5). For cryo measurements, crystals were transferred from the crystallization drop to the mother liquor supplied with 20% 2-methyl-2,4-pentanediol (OPR3) and 30–35% glycerol (OPR1 and OPR3YY) as cryoprotectant and rapidly frozen in a 100 K stream of nitrogen gas.

Structure solution and refinement

High-resolution data of OPR3 and OPR1 complexed with PHB were collected at the European Synchrotron Radiation Facility synchrotron (beamline ID14-4, $\lambda = 0.9393$ Å) using a Q4R ADSC CCD detector. Data were integrated using DENZO and scaled with SCALEPACK.[30] The crystal structures of the OPR1:PHB and OPR3:PHB complexes and of the OPR3YY double mutant were solved by molecular replacement using the program AMoRe[31] and the uncomplexed structures of OPR1 and OPR3 as search models. Energy-restrained crystallographic refinement was carried out with maximum likelihood algorithms implemented in CNS[32] using the protein parameters of Engh and Huber.[33] Refinement, model rebuilding with the program O,[34] and water incorporation proceeded smoothly via rigid-body, positional, and later *B*-factor optimization. The entire structure was checked with simulated annealing composite omit maps. The FMN cofactor, the PHB ligands, and the mutated residues were not included in the model during the first cycles of refinement; thereafter, they could be easily built into the clearly defined electron density. With the exception of 6–10 N-terminal and 11–12 C-terminal residues as well as 8–14 residues of loop L6, all OPR1 and OPR3 residues could be traced in the electron density map and exhibited good stereochemistry (Table 1). All parameter and topology files were generated with the program XPLO2D[35] and graphical presentations were prepared with MOLSCRIPT,[36] GRASP,[37] and Raster3D.[38] The amino acid sequence alignment was produced with CLUSTALW[39,40] and depicted with ALSCRIPT.[41]

Analysis of stereospecificity in OPR3 mutants

The activity of OPR3 and the site-directed mutants (Phe74Tyr, His244Tyr, Phe74Tyr/His244Tyr—OPR3; 1 μg each) with (9*S*,13*S*)-OPDA (0.1 mM) as the substrate was monitored over time. The reaction was performed in a total volume of 1 ml in the presence of 1 mM NADPH at pH 7.5 (100 mM phosphate buffer). At the indicated time points (Fig. 4), the reaction was stopped by acidification (HCl; pH<3) and the formation of DH-OPDA was analyzed by gas chromatography–mass spectrometry (GC–MS) according to Zerbe *et al.*[42] Briefly, DH-OPDA was extracted in diethylether, and the extract evaporated to dryness. After methylation, dried fractions were redissolved in 100 μl of chloroform, and 1 μl of the sample was injected into a Varian GC 3400 gas chromatograph (Varian, Darmstadt, Germany) in splitless mode in direct connection to a MAT Magnum ion-trap mass spectrometer (Finnigan, Bremen, Germany) using a chemical ionization mode with methanol as reactant gas. A ZB-35 fused silica capillary column (Phenomenex, Aschaffenburg, Germany; 30 m×0.25 mm×0.25 μm film thickness) with He carrier gas at 1 ml/min (gas pre-pressure of 80 kPa) was used for separation using the following temperature program: injector temperature of 260 °C, 1 min isothermally at 50 °C, with 20 °C/min up to 250 °C, 10 min isothermally at 250 °C, transferline temperature 260 °C.

For analysis of stereoselectivity, varying amounts of enzyme (1–100 μg) were analyzed with 0.2 mM of racemic mixture of (9*S*,13*S*)-OPDA and (9*R*,13*R*)-OPDA as the substrate under the same reaction conditions. The reaction was terminated after 30 min and residual substrate enantiomers were analyzed by GC–MS as described by Laudert *et al.* and Schaller *et al.* using a β-Dex120 column (30 m×0.25 mm×0.15 μm stationary-phase thickness) coated with 20% permethyl-β-cyclodextrin in SPB-35 (Supelco, Deisenhofen, Germany) with He carrier gas at 1 ml/min (gas pre-pressure of 80 kPa).[43,44] At all protein concentrations used for activity measurements, OPR3 was predominantly monomeric and therefore fully active.

Accession numbers

Coordinates and structure factors of OPR3YY, OPR1/PHB, and OPR3/PHB have been deposited in the Protein

Data Bank with accession numbers 3HGO, 3HGR, and 3HGS, respectively.

Acknowledgements

The Research Institute of Molecular Pathology (IMP) is funded by Boehringer Ingelheim, and T.C. was supported by the EMBO Young Investigator Program.

Supplementary Data

Supplementary data associated with this article can be found, in the online version, at doi:10.1016/j.jmb.2009.07.087

References

1. Massey, V. (2000). The chemical and biological versatility of riboflavin. *Biochem. Soc. Trans.* **28**, 283–296.
2. Williams, R. E. & Bruce, N. C. (2002). 'New uses for an old enzyme'—the old yellow enzyme family of flavoenzymes. *Microbiology*, **148**, 1607–1614.
3. Vick, B. A. & Zimmerman, D. C. (1984). Biosynthesis of jasmonic acid by several plant species. *Plant Physiol.* **75**, 458–461.
4. Schaller, F., Schaller, A. & Stintzi, A. (2004). Biosynthesis and metabolism of jasmonates. *J. Plant Growth Regul.* **23**, 179–199.
5. Wasternack, C. (2007). Jasmonates: an update on biosynthesis, signal transduction and action in plant stress response, growth and development. *Ann. Bot. (Lond)*, **100**, 681–697.
6. Stintzi, A. & Browse, J. (2000). The *Arabidopsis* male-sterile mutant, opr3, lacks the 12-oxophytodienoic acid reductase required for jasmonate synthesis. *Proc. Natl Acad. Sci. USA*, **97**, 10625–10630.
7. Stintzi, A., Weber, H., Reymond, P., Browse, J. & Farmer, E. E. (2001). Plant defense in the absence of jasmonic acid: the role of cyclopentenones. *Proc. Natl Acad. Sci. USA*, **98**, 12837–12842.
8. Schaller, F., Biesgen, C., Müssig, C., Altmann, T. & Weiler, E. W. (2000). 12-Oxophytodienoate reductase 3 (OPR3) is the isoenzyme involved in jasmonate biosynthesis. *Planta*, **210**, 979–984.
9. Strassner, J., Schaller, F., Frick, U. B., Howe, G. A., Weiler, E. W., Amrhein, N. *et al.* (2002). Characterization and cDNA-microarray expression analysis of 12-oxophytodienoate reductases reveals differential roles for octadecanoid biosynthesis in the local *versus* the systemic wound response. *Plant J.* **32**, 585–601.
10. Tani, T., Sobajima, H., Okada, K., Chujo, T., Arimura, S., Tsutsumi, N. *et al.* (2008). Identification of the OsOPR7 gene encoding 12-oxophytodienoate reductase involved in the biosynthesis of jasmonic acid in rice. *Planta*, **227**, 517–526.
11. Breithaupt, C., Strassner, J., Breitinger, U., Huber, R., Macheroux, P., Schaller, A. & Clausen, T. (2001). X-ray structure of 12-oxophytodienoate reductase 1 provides structural insight into substrate binding and specificity within the family of OYE. *Structure*, **9**, 419–429.
12. Breithaupt, C., Kurzbauer, R., Lilie, H., Schaller, A., Strassner, J., Huber, R. *et al.* (2006). Crystal structure of 12-oxophytodienoate reductase 3 from tomato: self-inhibition by dimerization. *Proc. Natl Acad. Sci. USA*, **103**, 14337–14342.
13. Fox, B. G., Malone, T. E., Johnson, K. A., Madson, S. E., Aceti, D., Bingman, C. A. *et al.* (2005). X-ray structure of *Arabidopsis* At1g77680, 12-oxophytodienoate reductase isoform 1. *Proteins*, **61**, 206–208.
14. Malone, T. E., Madson, S. E., Wrobel, R. L., Jeon, W. B., Rosenberg, N. S., Johnson, K. A. *et al.* (2005). X-ray structure of *Arabidopsis* At2g06050, 12-oxophytodienoate reductase isoform 3. *Proteins: Struct., Funct., Bioinf.* **58**, *243–245.*
15. Massey, V. & Schopfer, L. M. (1986). Reactivity of old yellow enzyme with alpha-NADPH and other pyridine-nucleotide derivatives. *J. Biol. Chem.* **261**, 1215–1222.
16. Niino, Y. S., Chakraborty, S., Brown, B. J. & Massey, V. (1995). A new old yellow enzyme of *Saccharomyces cerevisiae*. *J. Biol. Chem.* **270**, 1983–1991.
17. Meah, Y. & Massey, V. (2000). Old yellow enzyme: stepwise reduction of nitro-olefins and catalysis of aci-nitro tautomerization. *Proc. Natl Acad. Sci. USA*, **97**, 10733–10738.
18. Fox, K. M. & Karplus, P. A. (1994). Old yellow enzyme at 2-angstrom resolution—overall structure, ligand-binding, and comparison with related flavoproteins. *Structure*, **2**, 1089–1105.
19. Abramovitz, A. S. & Massey, V. (1976). Interaction of phenols with old yellow enzyme—physical evidence for charge-transfer complexes. *J. Biol. Chem.* **251**, 5327–5336.
20. Strassner, J., Fürholz, A., Macheroux, P., Amrhein, N. & Schaller, A. (1999). A homolog of old yellow enzyme in tomato—spectral properties and substrate specificity of the recombinant protein. *J. Biol. Chem.* **274**, 35067–35073.
21. Hall, M., Stueckler, C., Ehammer, C., Pointner, E., Oberdorfer, G., Gruber, K. *et al.* (2008). Asymmetric bioreduction of C=C bonds using enoate reductases OPR1, OPR3 and YqjM: enzyme-based stereocontrol. *Adv. Synth. Catal.* **350**, 411–418.
22. Sobajima, H., Takeda, M., Sugimori, M., Kobashi, N., Kiribuchi, K., Cho, E. M. *et al.* (2003). Cloning and characterization of a jasmonic acid-responsive gene encoding 12-oxophytodienoic acid reductase in suspension-cultured rice cells. *Planta*, **216**, 692–698.
23. Matsui, H., Nakamura, G., Ishiga, Y., Toshima, H., Inagaki, Y., Toyoda, K. *et al.* (2004). Structure and expression of 12-oxophytodienoate reductase (subgroup I) genes in pea, and characterization of the oxidoreductase activities of their recombinant products. *Mol. Genet. Genomics*, **271**, 1–10.
24. Zhang, J., Simmons, C., Yalpani, N., Crane, V., Wilkinson, H. & Kolomiets, M. (2005). Genomic analysis of the 12-oxo-phytodienoic acid reductase gene family of *Zea mays*. *Plant Mol. Biol.* **59**, 323–343.
25. Agrawal, G. K., Tamogami, S., Han, O., Iwahashi, H. & Rakwal, R. (2004). Rice octadecanoid pathway. *Biochem. Biophys. Res. Commun.* **317**, 1–15.
26. Rensing, S. A., Lang, D., Zimmer, A. D., Terry, A., Salamov, A., Shapiro, H. *et al.* (2008). The *Physcomitrella* genome reveals evolutionary insights into the conquest of land by plants. *Science*, **319**, 64–69.
27. Hall, M., Stueckler, C., Kroutil, W., Macheroux, P. & Faber, K. (2007). Asymmetric bioreduction of activated alkenes using cloned 12-oxophytodienoate reductase isoenzymes OPR-1 and OPR-3 from

Lycopersicon esculentum (tomato): a striking change of stereoselectivity. *Angew. Chem., Int. Ed. Engl.* **46**, 3934–3937.
28. Stuermer, R., Hauer, B., Hall, M. & Faber, K. (2007). Asymmetric bioreduction of activated C=C bonds using enoate reductases from the old yellow enzyme family. *Curr. Opin. Chem. Biol.* **11**, 203–213.
29. Strassner, J., Fürholz, A., Schaller, F., Macheroux, P., Weiler, E. W., Amrhein, N. & Schaller, A. (1999). Overexpression and characterization of 12-oxophytodienoic acid reductase from tomato, a member of the OYE family. In *Flavins and Flavoproteins* (Ghisla, S., Kroneck, P., Macheroux, P. & Sund, H., eds), pp. 655–658, Agency for Scientific Publ., Berlin.
30. Otwinowsky, Z. & Minor, W. (1993). DENZO: *A Film Processing Program for Macromolecular Crystallography*. Yale University Press, New Haven, CT.
31. Navaza, J. (1994). Amore—an automated package for molecular replacement. *Acta Crystallogr., Sect. A: Found. Crystallogr.* **50**, 157–163.
32. Brunger, A. T., Adams, P. D., Clore, G. M., DeLano, W. L., Gros, P., Grosse-Kunstleve, R. W. *et al.* (1998). Crystallography & NMR system: a new software suite for macromolecular structure determination. *Acta Crystallogr., Sect. D: Biol. Crystallogr.* **54**, *905–921.*
33. Engh, R. A. & Huber, R. (1991). Accurate bond and angle parameters for x-ray protein-structure refinement. *Acta Crystallogr., Sect. A: Found. Crystallogr.* **47**, *392–400.*
34. Jones, T. A., Zou, J. Y., Cowan, S. W. & Kjeldgaard, M. (1991). Improved methods for building protein models in electron-density maps and the location of errors in these models. *Acta Crystallogr., Sect. A: Found. Crystallogr.* **47**, *110–119.*
35. Kleywegt, G. J. & Jones, T. A. (1997). Model building and refinement practice. *Methods Enzymol.* **277**, 208–230.
36. Kraulis, P. J. (1991). Molscript—a program to produce both detailed and schematic plots of protein structures. *J. Appl. Crystallogr.* **24**, 946–950.
37. Nicholls, A., Sharp, K. A. & Honig, B. (1991). Protein folding and association—insights from the interfacial and thermodynamic properties of hydrocarbons. *Proteins: Struct., Funct., Genet.* **11**, *281–296.*
38. Merritt, E. A. & Murphy, M. E. P. (1994). Raster3d version-2.0—a program for photorealistic molecular graphics. *Acta Crystallogr., Sect. D: Biol. Crystallogr.* **50**, *869–873.*
39. Thompson, J. D., Higgins, D. G. & Gibson, T. J. (1994). CLUSTAL W: improving the sensitivity of progressive multiple sequence alignment through sequence weighting, position-specific gap penalties and weight matrix choice. *Nucleic Acids Res.* **22**, 4673–4680.
40. Larkin, M. A., Blackshields, G., Brown, N. P., Chenna, R., McGettigan, P. A., McWilliam, H. *et al.* (2007). Clustal W and Clustal X version 2.0. *Bioinformatics*, **23**, 2947–2948.
41. Barton, G. J. (1993). ALSCRIPT: a tool to format multiple sequence alignments. *Protein Eng.* **6**, 37–40.
42. Zerbe, P., Weiler, E. W. & Schaller, F. (2007). Preparative enzymatic solid phase synthesis of *cis* (+)-12-oxo-phytodienoic acid—physical interaction of AOS and AOC is not necessary. *Phytochemistry*, **68**, 229–236.
43. Laudert, D., Hennig, P., Stelmach, B. A., Muller, A., Andert, L. & Weiler, E. W. (1997). Analysis of 12-oxo-phytodienoic acid enantiomers in biological samples by capillary gas chromatography mass spectrometry using cyclodextrin stationary phases. *Anal. Biochem.* **246**, 211–217.
44. Schaller, F., Hennig, P. & Weiler, E. W. (1998). B12-oxophytodienoate-10,11-reductase: occurrence of two isoenzymes of different specificity against stereoisomers of 12-oxophytodienoic acid. *Plant Physiol.* **118**, 1345–1351.